scientific reports

Check for updates

OPEN

Magnetic silica/graphene oxide nanocomposite supported ionic liquid–manganese complex as a powerful catalyst for the synthesis of tetrahydrobenzopyrans

Farkhondeh Dadvar & Dawood Elhamifar✉

A novel magnetic silica/graphene oxide nanocomposite supported ionic liquid/manganese complex (Fe_3O_4@SiO_2-NH_2/GO/IL-Mn) is prepared, characterized and its catalytic application is investigated. The Fe_3O_4@SiO_2-NH_2/GO/IL-Mn catalyst was synthesized via chemical immobilization of graphene oxide on Fe_3O_4@SiO_2 nanoparticles followed by modification with ionic liquid/Mn complex. This nanocomposite was characterized by using SEM, TGA, FT-IR, PXRD, EDX, TEM, nitrogen adsorption–desorption, and VSM analyses. The catalytic application of Fe_3O_4@SiO_2-NH_2/GO/IL-Mn was studied in the synthesis of tetrahydrobenzo[b]pyrans (THBPs) in water solvent at RT. This nanocatalyst was successfully recovered and reused at least eight times without a significant decrease in its activity.

Carbon-based materials are very attractive among chemists due to their high efficiency as a support for different catalysts and also their good conductivity[1–3]. One of the most important allotropes of carbon is graphene oxide (GO)[4,5] which has a two-dimensional and single-layer structure and involves hydroxyl, carboxylic acid, and epoxy groups on its surface[6,7]. The properties of graphene oxides, such as very good specific surface area, biocompatibility, high flexibility, and lightness, endow them with strong potential for applications in catalytic processing[8–10]. However, GO accumulates in salt solutions and biological media. Therefore, to overcome this problem and also for easy separation of GO, recently, the immobilization of graphene oxide on magnetic nanoparticles has been considered[11,12]. In fact, the unique properties of magnetic NPs such as high surface area, availability, easy separation, and recoverability from the environment, make them attractive candidates to composite with GO. Some reports in this matter are TiO_2/Fe_3O_4/GO[13], Ag_3PO_4-Fe_3O_4-GO[14], PEG/Fe_3O_4/GO-NH_2[15], Fe_3O_4/GO-COOH[16], Fe_3O_4/GO/CS[17], MOF@Fe_3O_4@GO[18], Fe_3O_4-GO-(o-MWCNTs)hybrid[19], Fe_3O_4/GO/chitosan[20] and γ-PGA-Fe_3O_4-GO-(o-MWCNTs)[21]. Moreover, several organic functional groups have also been used to modify GO for practical applications[22]. Some reported examples in this matter are GO@IL/$MoO_2(acac)_2$[23], Cu–NiAAPTMS@GO[24], GO@melamine[25], plydopamine@GO/cellulose[26], Al_2O_3/GO cellulose[27], GO-TCT-DETA[28], and Mn-UiO-66@GO-NH_2[29].

An important process in chemistry is multicomponent reaction (MCR), in which at least three starting materials are used to synthesis valuable organic compounds[30–32]. As example, this process has been effectively used for the synthesis of tetrahydrobenzo[b]pyrans (THBPs)[33,34] with excellent biological activities such as antiviral, anticancer, and dementia[35,36]. Although, to date, many catalytic systems have been used for the synthesis of THBPs, however, the most of them suffer from drawbacks of high catalyst loading, the use of toxic organic solvents, high reaction temperature, and non-recoverability of the catalyst. Therefore, the preparation of a novel and powerful catalytic system to overcome the aforementioned limitations is an important challenge in this matter.

In view of the above, herein, we report the synthesis and characterization of a novel magnetic silica/graphene oxide nanocomposite supported ionic liquid/Mn complex (Fe_3O_4@SiO_2-NH_2/GO/IL-Mn). This is effectively applied as an efficient and recoverable catalyst in the synthesis of THBPs.

Department of Chemistry, Yasouj University, Yasouj 75918-74831, Iran. ✉email: d.elhamifar@yu.ac.ir

Experimental section

Preparation of Fe_3O_4@SiO_2-NH_2

For the synthesis of Fe_3O_4@SiO_2-NH_2, firstly, Fe_3O_4 nanoparticles were prepared according to a known method[37]. Then, 0.5 g of Fe_3O_4 was added in a solution containing 30 mL of ethanol, 20 mL of distilled water, and 10 mL of ammonia (25%). After that, 70 µL of 3-aminopropyltriethoxysilane (APTES) and 70 µL of tetraethoxysilane (TEOS) were added and the resulted mixture was stirred at 35 °C for 3 h. Finally, the product was separated by using a magnet, washed with distilled water and ethanol, dried at 75 °C for 7 h and denoted as Fe_3O_4@SiO_2-NH_2.

Preparation of Fe_3O_4@SiO_2-NH_2/GO

The Fe_3O_4@SiO_2-NH_2/GO nanocomposite was prepared as follows. First, 0.3 g of GO was suspended in 20 mL of distilled water for 10 min. Then, 0.5 g of Fe_3O_4@SiO_2-NH_2 was added and the obtained mixture was vigorously stirred at 70 °C for 2 h. Finally, the product was separated by using a magnet, washed with distilled water and ethanol, dried at 75 °C for 7 h and denoted as Fe_3O_4@SiO_2-NH_2/GO.

Preparation of Fe_3O_4@SiO_2-NH_2/GO/IL

For the preparation of Fe_3O_4@SiO_2-NH_2/GO/IL, firstly, 1 g of Fe_3O_4@SiO_2-NH_2/GO nanocomposite was suspended in 50 mL of toluene and sonicated for 20 min at RT. Then, 0.2 mmol of 1-methyl-3-(3-trimethoxysilylpropyl)imidazolium chloride (Im) was added and the obtained mixture was stirred under reflux conditions for 24 h. The product was separated by using a magnet, washed with ethanol, dried at 70 °C for 6 h and denoted as Fe_3O_4@SiO_2-NH_2/GO/IL.

Preparation of Fe_3O_4@SiO_2-NH_2/GO/IL-Mn

For this, 1 g of Fe_3O_4@SiO_2-NH_2/GO /IL was dispersed in 20 mL of DMSO under ultrasonic irradiation. Then, 0.5 mmol of $Mn(OAc)_3.4H_2O$ salt was added and the resulting mixture was stirred at 80 °C for 2 h. The product was separated by using a magnet, washed with ethanol, dried at 70 °C for 6 h and denoted as Fe_3O_4@SiO_2-NH_2/GO/IL-Mn.

Synthesis of THBPs using Fe_3O_4@SiO_2-NH_2/GO/IL-Mn nanocatalyst

For this purpose, the Fe_3O_4@SiO_2-NH_2/GO/IL-Mn catalyst (0.8 mol%), malononitrile (1 mmol), benzaldehyde (1 mmol) and dimedone (1 mmol) were added in distilled water (10 mL). The resulting mixture was vigorously stirred at RT. The progress of the reaction was monitored by using TLC. After the completion of the reaction, the catalyst was separated by using a magnet. Then, ethyl acetate (20 mL) was added to the residue and the obtained mixture was washed three times with water in a decanter to remove some impurities. Finally, the obtained ethyl acetate solution was placed in an ice bath to crystalize/precipitate the desired pure products.

IR, ^{1}H-NMR and ^{13}C-NMR data of THBPs

2-Amino-4-(3-nitrophenyl)-7,7-dimethyl-5-oxo-6,6,8,8-tetrahydro-4H-chromene-3-carbonitrile
White solid; yield: 85%; M. P.: 211–212 °C (210–212[35]), IR (KBr, cm^{-1}): 3420, 3339 (NH_2, stretching vibration), 3181 (=C–H, stretching vibration sp^2), 2958 (C–H, stretching vibration sp^3), 2186 (CN, stretching vibration), 1673 (C=O, stretching vibration), 1604, 1488 (C=C, Ar stretching vibration sp^2), 1245 (C–O, stretching vibration). ^{1}H-NMR (300 MHz, $CDCl_3$): δ (ppm) 0.99 (s, 3H), 1.09 (s, 3H), 2.15 (d, 1H, J = 15 Hz), 2.33 (d, 1H, J = 15 Hz), 2.59 (s, 2H), 4.46 (s, 1H), 7.24 (s, 2H), 7.63–7.75 (m, 2H), 8.2 (s, 1H), 8.3 (d, 1H, J = 9 Hz). ^{13}C-NMR (75 MHz, $CDCl_3$): δ (ppm) 27.6, 28.7, 32.5, 35.9, 40.4, 50.5, 56.9, 112.4, 120.1, 121.2, 122.3, 130.1, 134.8, 147.3, 148.7, 159.5, 164.1, 196.1.

2-Amino-4-(4-methylyphenyl)-7,7-dimethyl-5-oxo-6,6,8,8-tetrahydro-4Hchromene-3-carbonitrile.
White solid; yield: 85%; M. P.: 217–219 °C (218–220[38]), IR (KBr, cm^{-1}): 3424, 3328 (NH_2, stretching vibration), 3036 (=C–H, stretching vibration sp^2), 2960 (C–H, stretching vibration sp^3), 2192 (CN, stretching vibration), 1670 (C=O, stretching vibration), 1561, 1471 (C=C, Ar stretching vibration sp^2), 1241 (C–O, stretching vibration).^{1}H-NMR (300 MHz, CDCl3):1.08 (s, 3H), 1.15 (s, 3H), 2.10 (d, 1H, J = 6 MHz), 2.25 (d, 1H, J = 15.2 MHz), 2.25 (s, 3H), 2.52 (s, 2H), 4.43 (s, 1H), 7.05–7.14 (m, 4H), 7.28 (s, 2H) ^{13}C-NMR (75 MHz, CDCl3): δ (ppm) 21.2, 27.9, 29.1, 33.1, 35.1, 41.2, 50.9, 64.1, 114.2, 118.7, 127.5, 129.4, 137.0, 140.2, 157.4, 161.5, 196.0

2-Amino-4-(4-methoxyphenyl)-7,7-dimethyl-5-oxo-6,6,8,8-tetrahydro-4H-chromene-3-carbonitrile
White solid; yield: 90%; M. P.: 199–201 °C (196–198[39]), IR (KBr, cm^{-1}): 3432, 3332 (NH_2, stretching vibration), 3100 (=C–H, stretching vibration sp^2), 2958 (C–H, stretching vibration sp^3), 2190 (CN, stretching vibration), 1666 (C=O, stretching vibration), 1527, 1419 (C=C, Ar stretching vibration sp^2), 1249 (C–O, stretching vibration).^{1}H-NMR (300 MHz, CDCl3): δ (ppm) 1.05 (s,3H), 1.14 (s, 3H), 2.20 (d, 1H, J = 3.4 Hz), 2.23 (d, 1H, J = 3.4 Hz), 2.45 (s, 2H), 3.75 (s, 3H), 4.37 (s, 1H), 4.50 (s, 2H, NH2), 6.80 (d, 2H, J = 8.6 Hz), 7.15 (d, 2H, J = 8.6 Hz). ^{13}C NMR (75 MHz, CDCl3): δ (ppm) 27.8, 28.10, 32.4, 34.6, 40.6, 51.2, 63.9, 113.3, 114.6, 115.2, 128.8, 133.5, 135.3, 157.5, 158.4, 161.3, 195.9.

Results and discussion

The preparation of the Fe_3O_4@SiO_2-NH_2/GO/IL-Mn nanocomposite includes four steps (Fig. 1). Firstly, the magnetic Fe_3O_4 nanoparticles were modified with TEOS and APTES to give Fe_3O_4@SiO_2-NH_2 NPs. Secondly, this material was chemically reacted with GO to give Fe_3O_4@SiO_2-NH_2/GO nanocomposite. Thirdly, the Im-based ionic liquid was chemically grafted on the surface of Fe_3O_4@SiO_2-NH_2/GO to deliver the Fe_3O_4@SiO_2-NH_2/

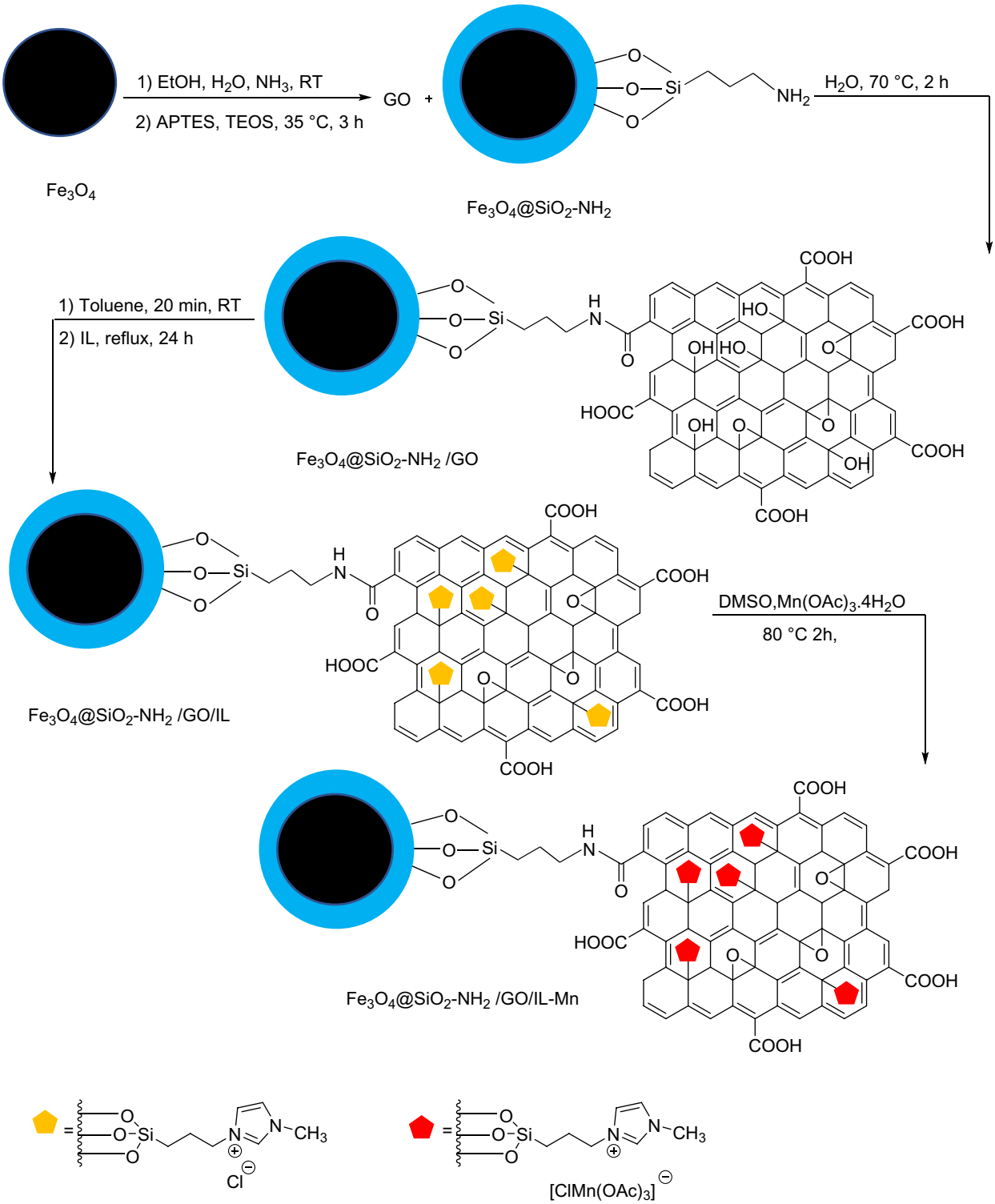

Figure 1. Preparation of the Fe_3O_4@SiO_2-NH_2/GO/IL-Mn nanocatalyst.

GO/IL material. Finally, the last product was treated with manganese acetate to give the Fe_3O_4@SiO_2-NH_2/GO/IL-Mn nanocatalyst.

The functional groups of the GO, Fe_3O_4@SiO_2-NH_2 and Fe_3O_4@SiO_2-NH_2/GO/IL-Mn materials were determined by using a Fourier transform infrared (FT-IR) spectrometer (Fig. 2). For all samples, the strong peak at 3394 cm^{-1} is due to the O–H bonds of the material surface (Fig. 2a–c)[40]. Moreover, the peaks at 1724, 1519, 1288 and 1049 cm^{-1} are, respectively, associated to carboxyl C=O, aromatic C=C, epoxy C–O and alkoxy C–O bonds of GO (Fig. 2a–c)[41]. For the Fe_3O_4@SiO_2-NH_2 and Fe_3O_4@SiO_2-NH_2/GO/IL-Mn materials, the signals

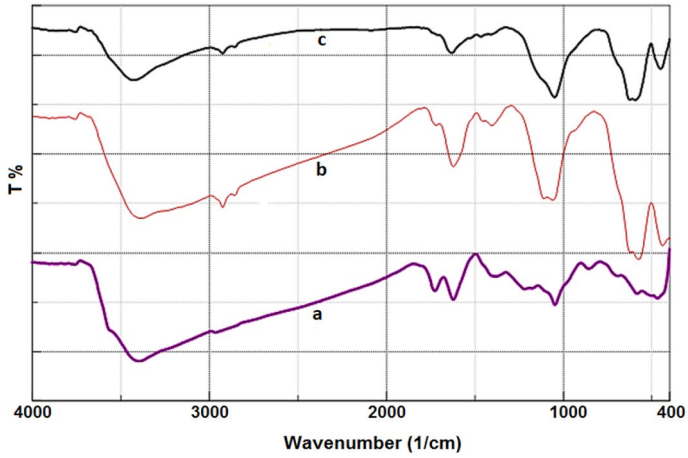

Figure 2. FT-IR spectra of (a) GO, (b) $Fe_3O_4@SiO_2$-NH_2 and (c) $Fe_3O_4@SiO_2$-NH_2/GO/IL-Mn.

at 2825 and 2923 cm^{-1} are attributed to the C–H bonds of the aliphatic groups (Fig. 2b and c)[42]. Moreover, for the latter materials, the peak at 593 cm^{-1} is assigned to the Fe–O bond (Fig. 2b and c)[43]. For $Fe_3O_4@SiO_2$-NH_2/GO/IL-Mn, the signal at 1627 cm^{-1} is attributed to C=N bond of ionic liquids (Fig. 2c)[41,44]. In addition, for both $Fe_3O_4@SiO_2$-NH_2 and $Fe_3O_4@SiO_2$-NH_2/GO/IL-Mn nanomaterials, the strong signals at 1083 and 1215 cm^{-1} are assigned to the Si–O-Si vibrations[45,46].

The surface morphology of $Fe_3O_4@SiO_2$-NH_2/GO/IL-Mn was studied by using SEM technique. The spherical nanoparticles of $Fe_3O_4@SiO_2$ NPs and also the graphene oxide layers were clearly seen in the SEM image (Fig. 3). This confirms the successful formation of the $Fe_3O_4@SiO_2$-NH_2/GO composite during applied conditions.

The TEM analysis of the designed catalyst was also performed to investigate its structure. This analysis showed the catalyst to be composed of spherical $Fe_3O_4@SiO_2$ NPs and GO layers (Fig. 4).

The EDX analysis showed the signals of carbon, nitrogen, oxygen, silicon, manganese and iron elements in the prepared nanocomposite (Fig. 5). This is in good agreement with the FT-IR results, confirming the successful immobilization of IL-Mn complex on $Fe_3O_4@SiO_2$-NH_2/GO composite.

The EDX-mapping analysis of the $Fe_3O_4@SiO_2$-NH_2/GO/IL-Mn nanocatalyst is shown in Fig. 6. As seen, all desired elements of C, O, N, Fe, Si and Mn are very well distributed in the material. This is also in good agreement with the FT-IR and EDX results, indicating the successful formation of the designed $Fe_3O_4@SiO_2$-NH_2/GO/IL-Mn nanocomposite.

The powder XRD analysis of $Fe_3O_4@SiO_2$-NH_2/GO/IL-Mn showed six signals at 2θ of 30, 35.5, 43.1, 54, 57.2, and 63.5 degree, corresponding to the *Miller indices* of 220, 311, 400, 422, 511 and 440, respectively (Fig. 7). These signals are attributed to the spinel structure of magnetic iron oxide NPs,[47,48] confirming the high stability of the magnetite NPs during modification processes. Also, the peak at 2θ = 19° is related to silica layer of the designed catalyst[49,50].

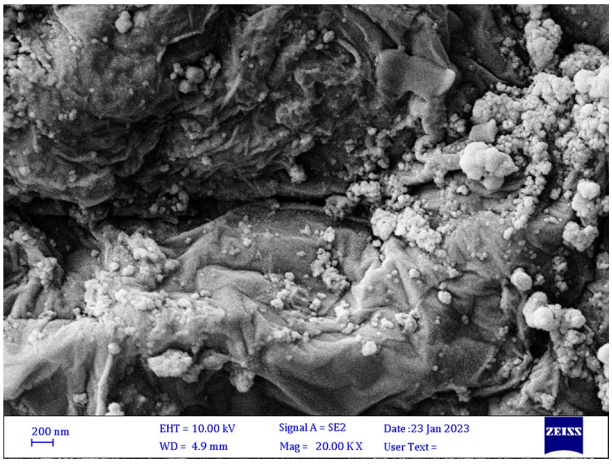

Figure 3. SEM image of $Fe_3O_4@SiO_2$-NH_2/GO/IL-Mn.

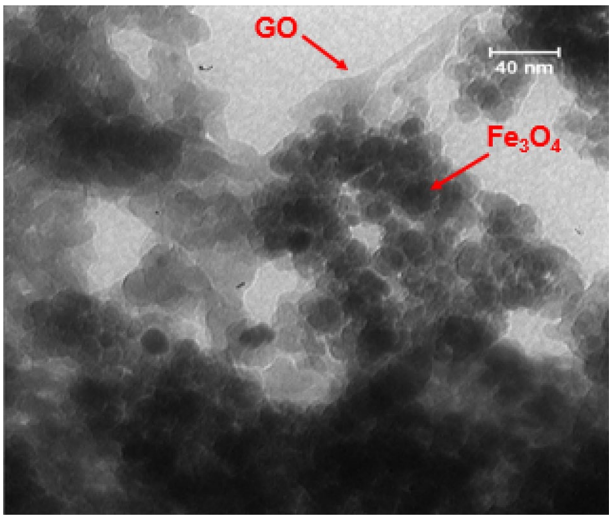

Figure 4. TEM image of Fe_3O_4@SiO_2-NH_2/GO/IL-Mn.

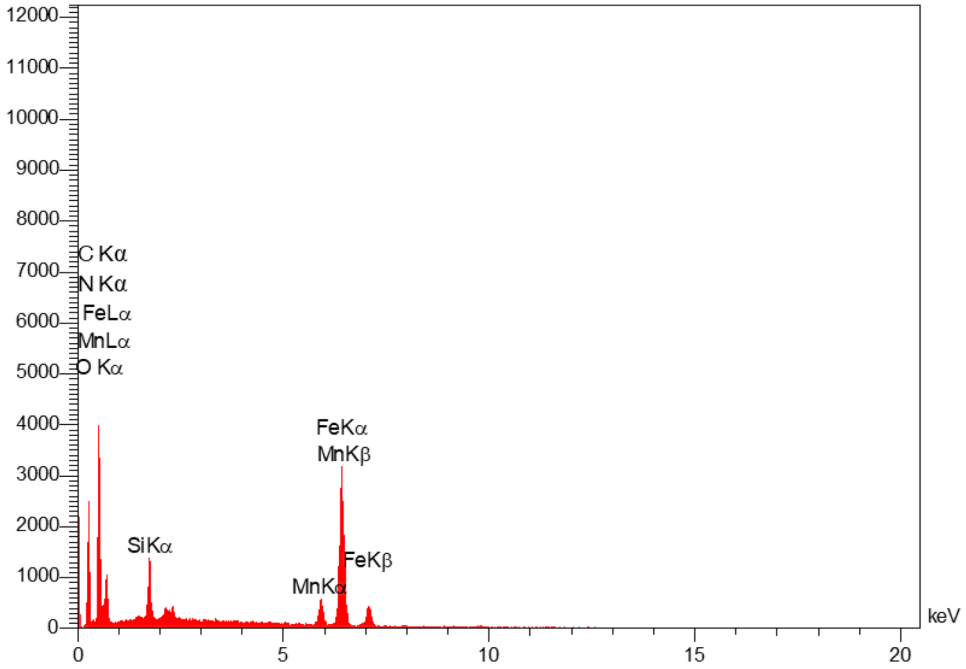

Figure 5. EDX analysis of Fe_3O_4@SiO_2-NH_2/GO/IL-Mn.

According to the VSM analysis, the saturation magnetization of the designed Fe_3O_4@SiO_2-NH_2/GO/IL-Mn material was found to be 40 emu/g (Fig. 8), confirming its high magnetic properties. This characteristic is very important in the fields of adsorption and catalysis.

Thermal stability of the Fe_3O_4@SiO_2-NH_2/GO/IL-Mn nanocatalyst was investigated by using thermal gravimetric analysis (TGA, Fig. 9). The first weight loss at temperatures between 10 to 110 °C (3%) is related to the removal of water and alcoholic solvents[39]. The second weight loss at 111–210 °C (4%) is attributed to the removal of the parts of functional groups that are located on the surface of the material. The main weight loss at temperatures more than 220 °C is related to the complete removal of the ionic liquids and also some parts of GO.

The nitrogen adsorption–desorption isotherms of the Fe_3O_4@SiO_2-NH_2/GO/IL-Mn nanocomposite showed a type II curve with a pronounced H3 hysteresis loop, according to the IUPAC classification[51]. The BET specific surface area and total pore volume of the material were calculated to be about 386.5 m^2/g and 0.35 cm^3/g, respectively. In addition, the BJH pore size distribution analysis showed a peak with good intensity centered at average pore diameter of about 4.8 nm (Fig. 10).

After preparation and characterization, the catalytic activity of Fe_3O_4@SiO_2-NH_2/GO/IL-Mn was investigated in the synthesis of THBPs at room temperature (RT). For this, the reaction between benzaldehyde, dimedone and

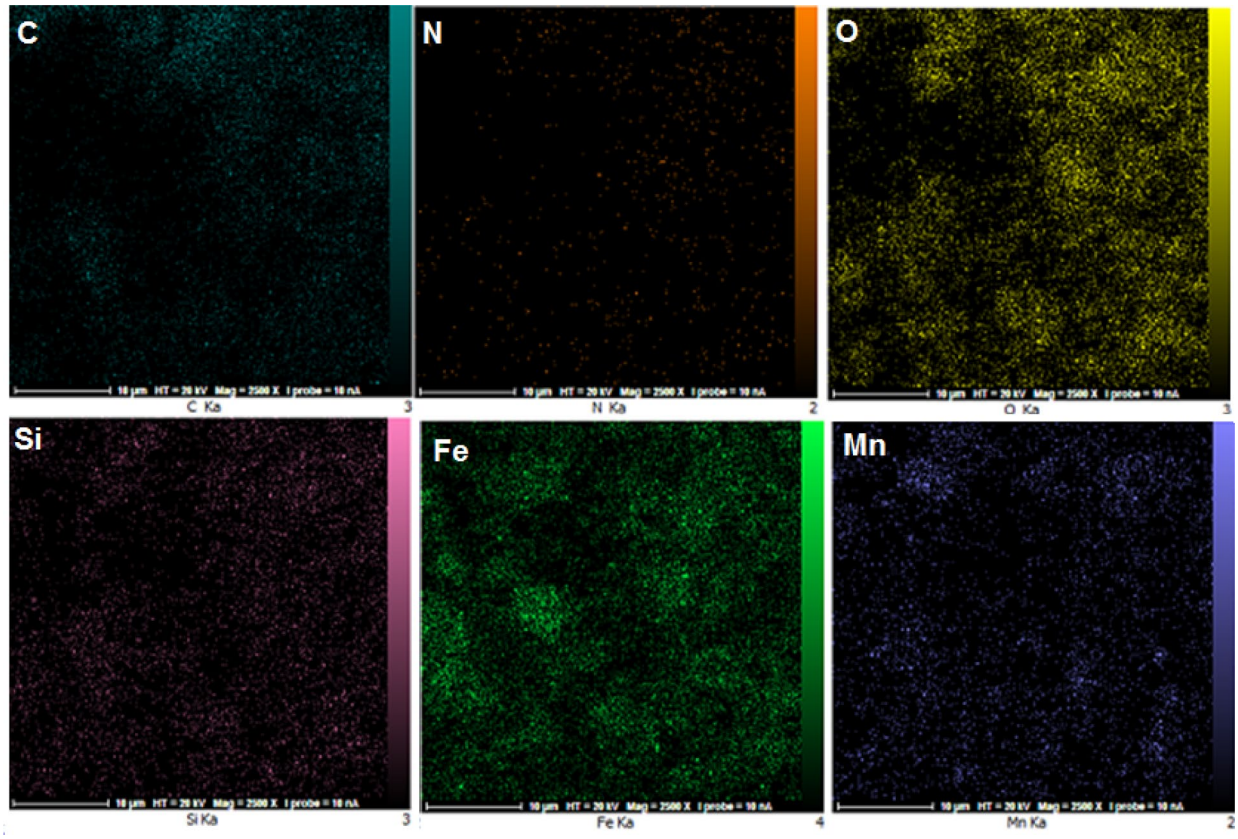

Figure 6. EDX-mapping analysis of the Fe_3O_4@SiO_2-NH_2/GO/IL-Mn nanocatalyst.

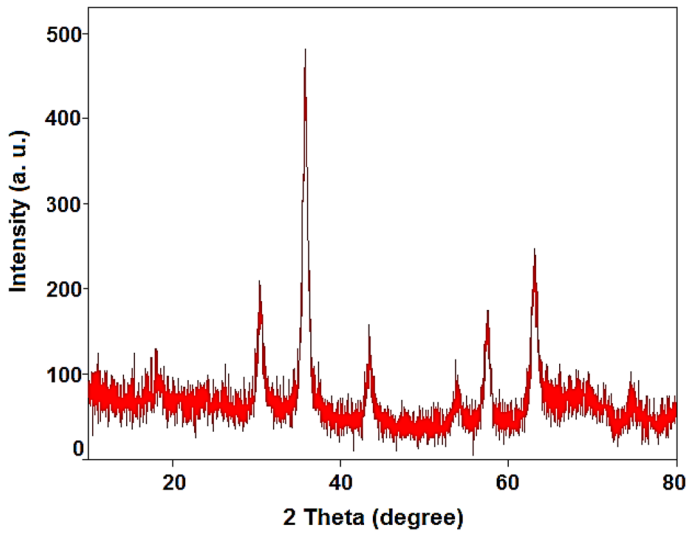

Figure 7. PXRD pattern of the Fe_3O_4@SiO_2-NH_2/GO/IL-Mn nanocatalyst.

malononitrile was selected as a test model (Table 1). The effect of various parameters such as catalyst loading and solvent was investigated to obtain the best conditions. In the absence of a catalyst, no product was obtained after 3 h, proving the catalyst is necessary for the development of this reaction (Table 1, entry 1). After addition of the catalyst, the reaction was progressed effectively and the best result was obtained in the presence of 0.8 mol% of Fe_3O_4@SiO_2-NH_2/GO/IL-Mn (Table 1, entries 2–4). It is important to note that increasing the amount catalyst to 1 mol% did not result in a significant change in the reaction yield (Table 1, entry 5). In order to demonstrate the effect of the Mn-centers on the catalytic process, the catalytic activity of Mn-free Fe_3O_4@SiO_2-NH_2/GO/IL nanocomposite was also investigated. This experiment showed that the Mn-free material gave no yield of the desired product, verifying the process is actually catalyzed by catalytic Mn sites (Table 1, entry 6). This catalytic

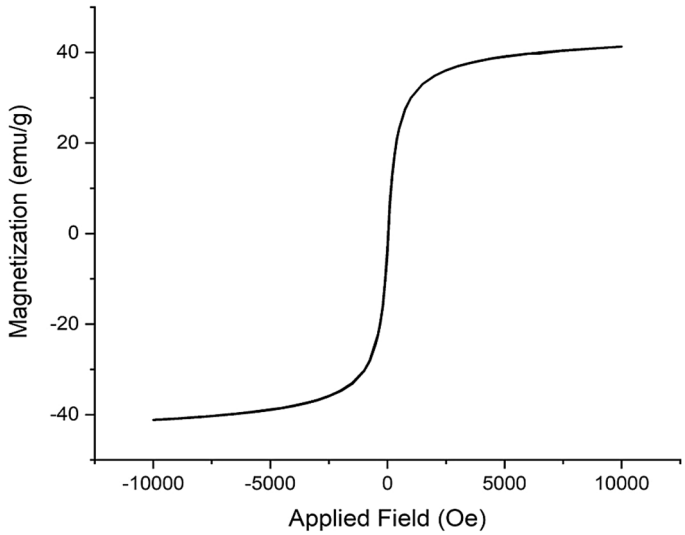

Figure 8. VSM of the Fe_3O_4@SiO_2-NH_2/GO/IL-Mn nanocatalyst.

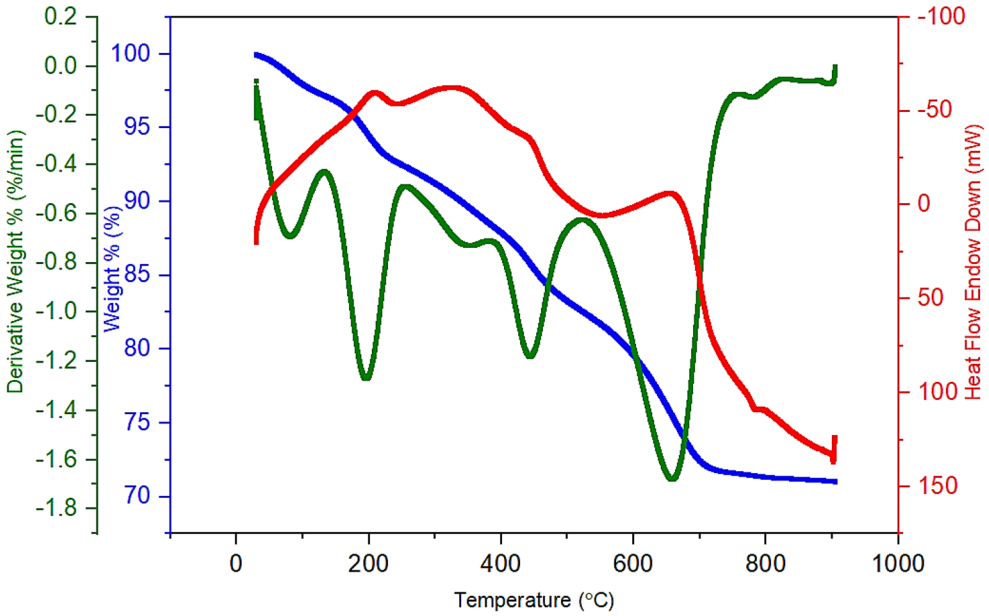

Figure 9. TGA of the Fe_3O_4@SiO_2-NH_2/GO/IL-Mn nanocatalyst.

system was also significantly affected by the solvent. Yields of 58%, 82%, 53% were obtained in toluene, EtOH and also under solvent-free media, respectively. Pleasingly, in water, the best yield was obtained (Table 1, entry 4). Accordingly, 0.8 mol% of catalyst, water solvent and RT were identified as the optimal conditions (Table 1, entry 4).

With the optimum conditions in hand, various aldehyde derivatives containing both electron withdrawing and electron donating substituents were used as substrate (Table 2). All of these aldehydes delivered the desired products in high yield at short time. It was also found that Fe_3O_4@SiO_2-NH_2/GO/IL-Mn offers high turnover number (TON) and turnover frequency (TOF) for all products, confirming the high ability of the present catalytic system to synthesis a wide range of biologically active THBPs.

The recoverability and reusability of Fe_3O_4@SiO_2-NH_2/GO/IL-Mn were also investigated in the reaction model. For this, after finishing of the reaction, the catalyst was easily separated by using a magnet. Then, it was reused in the next run under the same conditions as the first run. These steps were repeated and it was found that the catalyst could be recovered and reused for at least eight times with no significant decrease in efficiency (Fig. 11). These findings confirm high performance and very good stability of the designed catalyst under applied conditions.

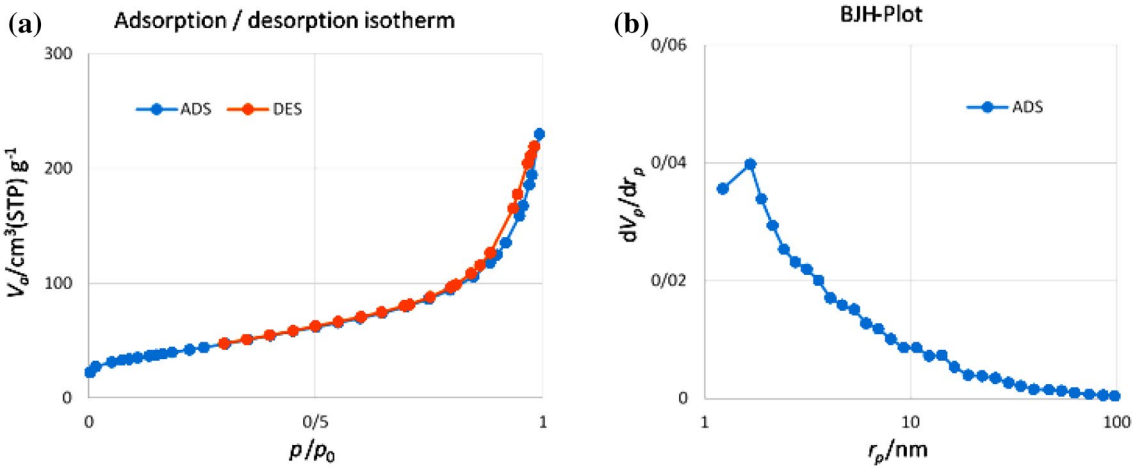

Figure 10. (**a**) Nitrogen adsorption–desorption and (**b**) BJH pore size distribution isotherms of the Fe_3O_4@SiO_2-NH_2/GO/IL-Mn nanocatalyst.

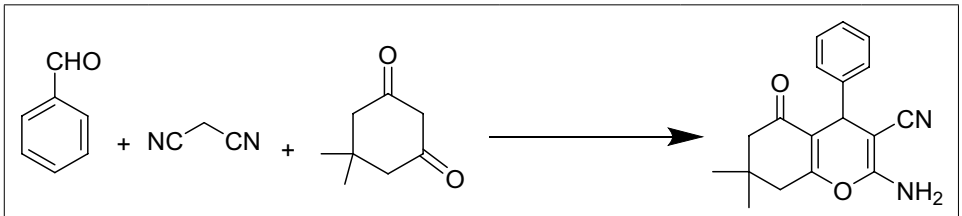

Entry	Catalyst (mol%)	Solvent	Time (min)	Yield (%)
1	–	H_2O	180	–
2	Fe_3O_4@SiO_2-NH_2/GO/IL-Mn (0.4)	H_2O	40	43
3	Fe_3O_4@SiO_2-NH_2/GO/IL-Mn (0.6)	H_2O	40	72
4	Fe_3O_4@SiO_2-NH_2/GO/IL-Mn (0.8)	H_2O	40	95
5	Fe_3O_4@SiO_2-NH_2/GO/IL-Mn (1)	H_2O	40	96
6	Fe_3O_4@SiO_2-NH_2/GO/IL (0.01 g)	H_2O	40	12
7	Fe_3O_4@SiO_2-NH_2/GO/IL-Mn (0.8)	Toluene	40	58
8	Fe_3O_4@SiO_2-NH_2/GO/IL-Mn (0.8)	EtOH	40	82
9	Fe_3O_4@SiO_2-NH_2/GO/IL-Mn (0.8)	Solvent-free	40	53

Table 1. Effect of solvent and catalyst loading in the synthesis of THBPs at RT.

Next, a leaching test was performed in the model reaction to investigate the nature of the Fe_3O_4@SiO_2-NH_2/GO/IL-Mn nanocatalyst under the applied conditions. For this, after the conversion was about 45% complete, the catalyst was magnetically removed. Then, the progress of catalyst-free residue was monitored. Interestingly, after 120 min, no notable conversion was observed. This proves no leaching of Mn species in the reaction solution under the applied conditions and also the heterogeneous nature of the designed catalyst.

Furthermore, the reactivity of the catalyst was investigated under optimal conditions. For this purpose, the model reaction was carried out and its progress was monitored using TLC. After the completion of the reaction, the starting materials were again added to the reaction vessel in the same proportion as the first run. These steps were repeated and the results showed that the activity of the Fe_3O_4@SiO_2-NH_2/GO/IL-Mn nanocatalyst is maintained for at least seven runs without a significant decrease in performance (Table 3).

In the next, in order to study the chemical and structural stability of the catalyst under applied conditions, the FT-IR and XRD analyses of the recovered catalyst were performed after fifth run. As shown in Fig. 12, the FT-IR spectrum of the recovered Fe_3O_4@SiO_2-NH_2/GO/IL-Mn showed a pattern similar to the FT-IR of fresh nanocatalyst, proving the high stability of the designed material under the applied reaction conditions.

The PXRD of the recovered Fe_3O_4@SiO_2-NH_2/GO/IL-Mn also illustrated six peaks at 2θ of 30, 35.5, 43.1, 54, 57.2, and 63.5, which are in good agreement with the PXRD pattern of the fresh nanocatalyst, proving the high stability of the crystalline structure of Fe_3O_4 NPs during the reaction process (Fig. 13).

Finally, the performance of Fe_3O_4@SiO_2-NH_2/GO/IL-Mn nanocomposite was compared with some previous catalytic systems in the synthesis of THBPs (Table 4). The results showed that our catalyst is better in terms of reaction conditions, catalyst loading and recovery times. These findings may be attributed to the magnetic

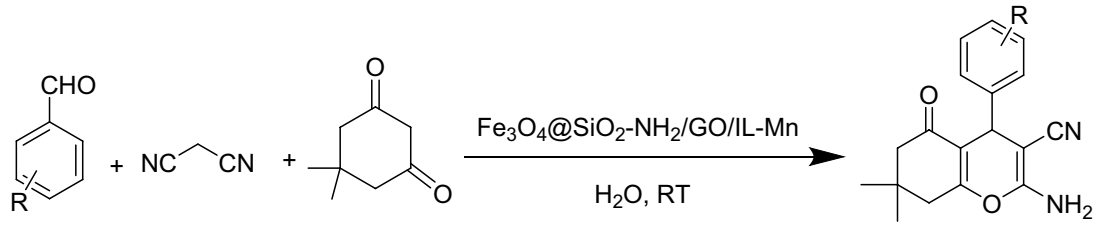

Entry	R	Time (min)	TON[a]	TOF[b]	Yield (%)	Found M. P. (°C)	Reported M. P. (°C)
1	H	40	118.75	179.92	95	221–224	222–224[52]
2	4-Cl	26	112.5	261.62	90	210–213	210–212[35]
3	4-OMe	35	112.5	193.96	90	199–201	196–198[39]
4	4-Me	37	106.25	174.18	85	217–219	218–220[38]
5	3-NO_2	20	106.25	321.97	85	211–212	210–212[35]
6	4-NO_2	15	110	440	88	181–183	182–184[35]

Table 2. Synthesis of THBPs in the presence of Fe_3O_4@SiO_2-NH_2/GO/IL-Mn at RT. [a]Turnover number [defined as yield (%)/cat. (mol%)]. [b]Turnover frequency [defined as TON/reaction time (h)].

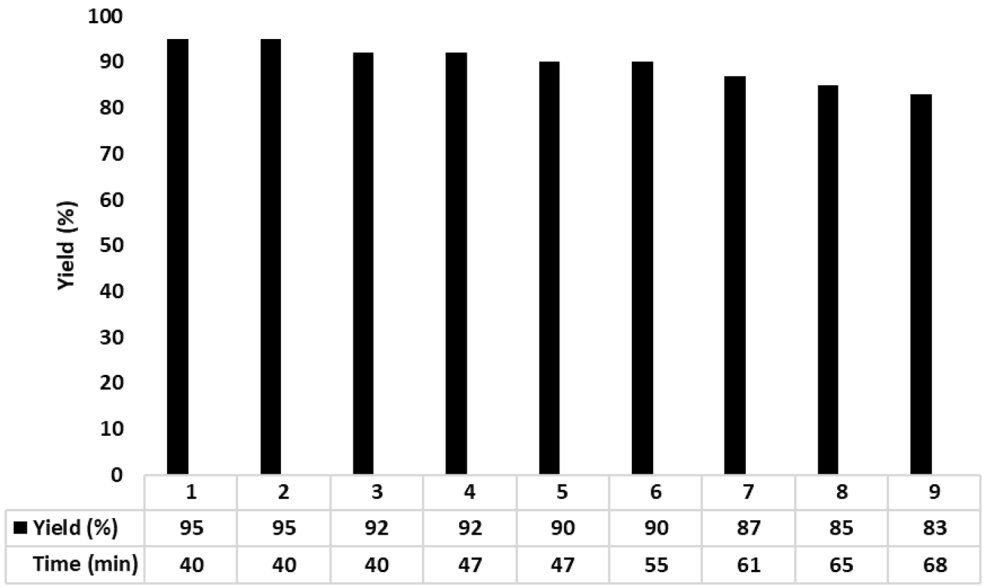

Figure 11. Recoverability and reusability of Fe_3O_4@SiO_2-NH_2/GO/IL-Mn.

Run	1	2	3	4	5	6	7	8
Time (min)	40	40	47	50	53	60	60	64

Table 3. Catalytic reactivity of the Fe_3O_4@SiO_2-NH_2/GO/IL-Mn nanocomposite.

nature of Fe_3O_4@SiO_2-NH_2/GO/IL-Mn as well as the positive effect of chemically immobilized ionic liquids in the stabilization of the catalytically active Mn-species.

A plausible mechanism for the synthesis of THBPs using Fe_3O_4@SiO_2-NH_2/GO/IL-Mn is outlined in Fig. 14. At first, the malononitrile and the Mn-activated aldehyde are condensed through the Knoevenagel condensation to give intermediate **1**. Intermediate **2** is then delivered via a Michael-type addition between the enol form of dimedone and intermediate **1**. An intramolecular cyclo-condensation is performed on intermediate **2** to give intermediate **3**. Finally, the intermediate **3** is converted to the desired product **4** through a tautomerization process[58].

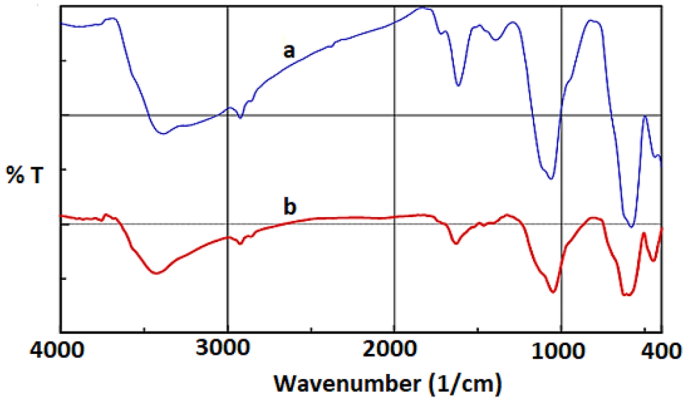

Figure 12. FT-IR spectra of (a) fresh Fe_3O_4@SiO_2-NH_2/GO/IL-Mn and (b) recovered Fe_3O_4@SiO_2-NH_2/GO/IL-Mn.

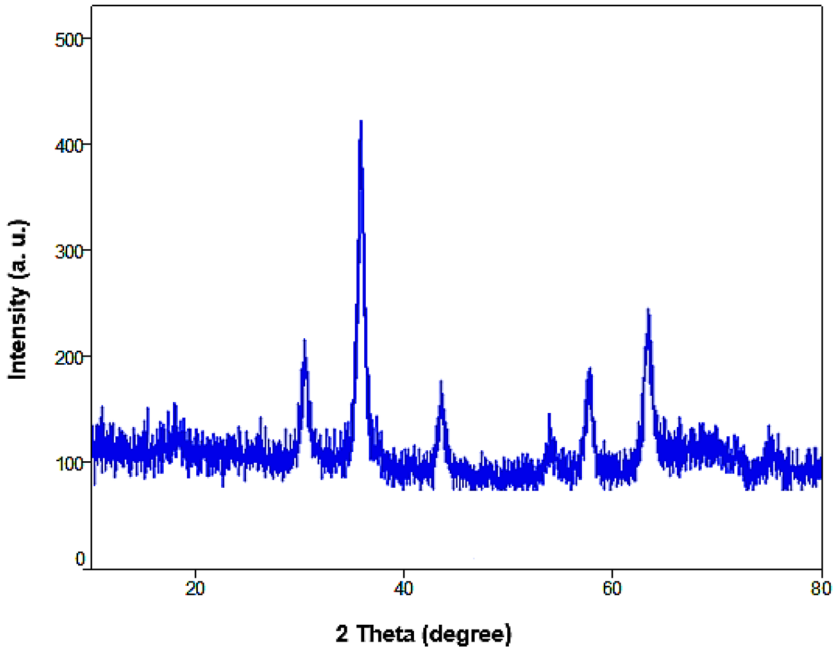

Figure 13. PXRD pattern of the recovered Fe_3O_4@SiO_2-NH_2/GO /IL-Mn nanocomposite.

Catalyst	Conditions	Recovery times	Ref.
MGO-D-NH-$(CH_2)_4$-SO_3H	Cat.0.02 g, H_2O/ethanol, 35 °C	6	[53]
Fe_3O_4@SiO_2@TiO_2	Cat. 0.01 g, solvent free, 100 °C	6	[54]
$[Et_3NH][HSO_4]$	Cat. 0.025 g, solvent free/MW	3	[55]
CaO@SiO_2-SO_3H	Cat. 0.02 g, H_2O/50 °C	6	[56]
GO–Si–NH_2–PMo	Cat. 0.04 g, solvent-free 90 °C	5	[57]
Fe_3O_4@SiO_2-NH_2/GO/IL-Mn	Cat. 0.8 mol%. H_2O/RT	8	This work

Table 4. The comparative study of Fe_3O_4@SiO_2-NH_2/GO/IL-Mn with previously reported catalysts.

Conclusion

In this study, for the first time, a manganese-containing IL-modified Fe_3O_4@SiO_2-NH_2/GO nanocomposite was prepared, characterized and used as a novel catalyst for the synthesis of THBPs. The high chemical and thermal stability of the designed catalyst were confirmed by using FT-IR, TGA and EDX analyses. The PXRD and VSM analyses showed high magnetic properties of the designed catalyst. The SEM and TEM analyses also confirmed

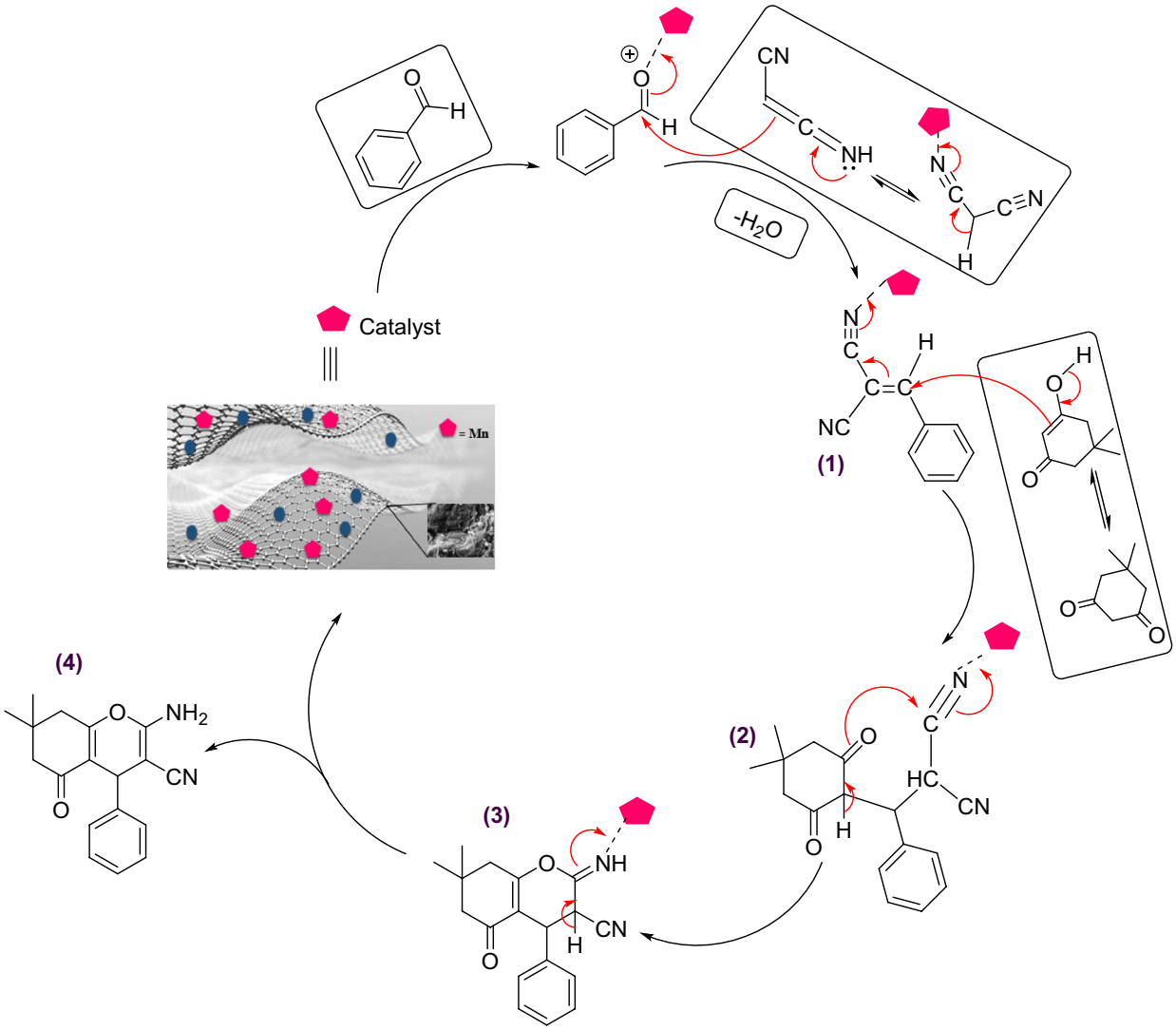

Figure 14. Proposed mechanism for the synthesis of THBPs using the Fe_3O_4@SiO_2-NH_2/GO/IL-Mn nanocomposite.

the successful formation of the Fe_3O_4@SiO_2-NH_2/GO composite. The Fe_3O_4@SiO_2-NH_2/GO/IL-Mn catalyst was effectively used in the synthesis of THBPs and gave the desired products in high yields. The leaching test and also the recoverability and reactivity studies clearly showed high performance and stability of the catalyst under applied conditions.

Data availability

All data and materials are included in the manuscript.

Received: 3 June 2023; Accepted: 3 November 2023
Published online: 07 November 2023

References

1. Zare, P., Aleemardani, M., Seifalian, A., Bagher, Z. & Seifalian, A. M. Graphene oxide: Opportunities and challenges in biomedicine. *Nanomaterials* **11**, 1083 (2021).
2. Liu, L. *et al.* Phase change materials with Fe_3O_4/GO three-dimensional network structure for acoustic-thermal energy conversion and management. *Chem. Eng. J.* **426**, 130789 (2021).
3. Darvishi, K., Amani, K. & Rezaei, M. Preparation, characterization and heterogeneous catalytic applications of GO/Fe_3O_4/HPW nanocomposite in chemoselective and green oxidation of alcohols with aqueous H_2O_2. *Appl. Organomet. Chem.* **32**, e4323 (2018).
4. Liu, C., Liu, Y., Dang, Z., Zeng, S. & Li, C. Enhancement of heterogeneous photo-Fenton performance of core-shell structured boron-doped reduced graphene oxide wrapped magnetical Fe_3O_4 nanoparticles: Fe (II)/Fe (III) redox and mechanism. *Appl. Surf. Sci.* **544**, 148886 (2021).
5. Liu, Z. *et al.* Fe_3O_4@ graphene oxide@ Ag particles for surface magnet solid-phase extraction surface-enhanced Raman scattering (SMSPE-SERS): From sample pretreatment to detection all-in-one. *ACS Appl. Mater. Interfaces* **8**, 14160–14168 (2016).
6. Yu, W., Sisi, L., Haiyan, Y. & Jie, L. Progress in the functional modification of graphene/graphene oxide: A review. *RSC Adv.* **10**, 15328–15345 (2020).

7. Seabra, A. B., Paula, A. J., de Lima, R., Alves, O. L. & Durán, N. Nanotoxicity of graphene and graphene oxide. *Chem. Res. Toxicol.* **27**, 159–168 (2014).
8. Agarwal, V. & Zetterlund, P. B. Strategies for reduction of graphene oxide—A comprehensive review. *Chem. Eng. J.* **405**, 127018 (2021).
9. Rao, C., Biswas, K., Subrahmanyam, K. & Govindaraj, A. Graphene, the new nanocarbon. *J. Mater. Chem.* **19**, 2457–2469 (2009).
10. Razaq, A. *et al.* Review on graphene-, graphene oxide-, reduced graphene oxide-based flexible composites: From fabrication to applications. *Materials* **15**, 1012 (2022).
11. Kumar, N. *et al.* Top-down synthesis of graphene: A comprehensive review. *FlatChem* **27**, 100224 (2021).
12. Tiwari, S. K., Sahoo, S., Wang, N. & Huczko, A. Graphene research and their outputs: Status and prospect. *J. Sci. Adv. Mater. Devices* **5**, 10–29 (2020).
13. Hamdy, G., El-Sabbagh, I. A. & Taher, F. Highly efficient sorption of thorium (IV) onto a ternary magnetic TiO_2/Fe_3O_4/GO nanocomposite. *Mater. Today Proc.* **42**, 2218–2226 (2021).
14. Muthukumar, P., Alex, V., Pannipara, M., Al-Sehemi, A. G. & Anthony, S. P. Fabricating highly efficient Ag_3PO_4-Fe_3O_4-GO ternary nanocomposite photocatalyst: Effect of Fe_3O_4-GO preparation methods on photocatalytic activity. *Mater. Res. Bull.* **141**, 111337 (2021).
15. He, L. *et al.* Removal of Ca^{2+} and Mg^{2+} from oilfield wastewater using reusable PEG/Fe_3O_4/GO-NH_2 nanoadsorbents and its efficiency for oil recovery. *J. Environ. Chem. Eng.* **9**, 104653 (2021).
16. He, L. *et al.* A reusable Fe_3O_4/GO-COOH nanoadsorbent for Ca^{2+} and Cu^{2+} removal from oilfield wastewater. *Chem. Eng. Res. Des.* **166**, 248–258 (2021).
17. John, J. A., Samuel, M. S. & Selvarajan, E. Immobilized cellulase on Fe_3O_4/GO/CS nanocomposite as a magnetically recyclable catalyst for biofuel application. *Fuel* **333**, 126364 (2023).
18. Jia, W., Du, A., Fan, Z. & Shi, L. Goat milk-derived short chain peptides: Peptide LPYV as species-specific characteristic and their versatility bioactivities by MOF@ Fe_3O_4@ GO mesoporous magnetic-based peptidomics. *Food Res. Int.* **164**, 112442 (2023).
19. Wang, L. *et al.* Anionic polypeptide poly (γ-glutamic acid)-functionalized magnetic Fe_3O_4-GO-(o-MWCNTs) hybrid nanocomposite for high-efficiency removal of Cd (II), Cu (II) and Ni (II) heavy metal ions. *Chem. Eng. J.* **346**, 38–49 (2018).
20. Yadav, M., Rhee, K. Y., Park, S. J. & Hui, D. Mechanical properties of Fe_3O_4/GO/chitosan composites. *Compos. Part B Eng.* **66**, 89–96 (2014).
21. Zhang, Q., Hou, Q., Huang, G. & Fan, Q. Removal of heavy metals in aquatic environment by graphene oxide composites: A review. *Environ. Sci. Pollut. Res.* **27**, 190–209 (2020).
22. Farjadian, F. *et al.* Recent developments in graphene and graphene oxide: Properties, synthesis, and modifications: A review. *ChemistrySelect* **5**, 10200–10219 (2020).
23. Kargar, S., Elhamifar, D. & Zarnegaryan, A. Ionic liquid modified graphene oxide supported Mo-complex: A novel, efficient and highly stable catalyst. *Surf. Interfaces* **23**, 100946 (2021).
24. Rana, S., Maddila, S. & Jonnalagadda, S. B. Synthesis and characterization of Pd (II) dispersed over diamine functionalized graphene oxide and its scope as a catalyst for selective oxidation. *Catal. Sci. Technol.* **5**, 3235–3241 (2015).
25. Chen, J. *et al.* Syntheses of magnetic GO@ melamine formaldehyde resin for dyes adsorption. *Mater. Res. Express* **6**, 086103 (2019).
26. Liu, Y. *et al.* Construction of a mesoporous polydopamine@ GO/cellulose nanofibril composite hydrogel with an encapsulation structure for controllable drug release and toxicity shielding. *ACS Appl. Mater. Interfaces* **12**, 57410–57420 (2020).
27. Singh, N., Kumari, S., Goyal, N. & Khan, S. Al_2O_3/GO cellulose based 3D-hydrogel for efficient fluoride removal from water. *Environ. Nanotechnol. Monit. Manag.* **15**, 100444 (2021).
28. Ma, L. *et al.* Reinforcing carbon fiber epoxy composites with triazine derivatives functionalized graphene oxide modified sizing agent. *Compos. Part B Eng.* **176**, 107078 (2019).
29. Eltaweil, A. S., Elshishini, H. M., Ghatass, Z. F. & Elsubruiti, G. M. Ultra-high adsorption capacity and selective removal of Congo red over aminated graphene oxide modified Mn-doped UiO-66 MOF. *Powder Technol.* **379**, 407–416 (2021).
30. Khumalo, M. R., Maddila, S. N., Maddila, S. & Jonnalagadda, S. B. A facile and one-pot synthesis of new tetrahydrobenzo [b] pyrans in water under microwave irradiation. *BMC Chem.* **13**, 1–7 (2019).
31. Hassanzadeh, F., Daneshvar, N., Shirini, F. & Mamaghani, M. Introduction of a new bis-derivative of succinimide (Bis-Su) as a sustainable and efficient basic organo-catalyst for the synthesis of arylidene malononitrile and tetrahydrobenzo [b] pyran derivatives under green conditions. *Res. Chem. Intermed.* **46**, 4971–4984 (2020).
32. Memar, F. O., Khazdooz, L., Zarei, A. & Abbaspourrad, A. Green synthesis of pyrano [3, 2-b] pyran derivatives using nano Si–Mg–fluorapatite catalyst and the evaluation of their antibacterial and antioxidant properties. *Med. Chem. Res.* **29**, 1792–1803 (2020).
33. Mohammadi, A. A., Asghariganjeh, M. R. & Hadadzahmatkesh, A. Synthesis of tetrahydrobenzo [b] pyran under catalysis of $NH_4Al(SO_4)_2 \cdot 12H_2O$ (Alum). *Arab. J. Chem.* **10**, S2213–S2216 (2017).
34. Badiger, K. B., Sannegowda, L. K. & Kamanna, K. Microwave-assisted one-pot synthesis of tetrahydrobenzo [b] pyrans in the presence of WEWFPA and their electrochemical studies. *Organ. Commun.* **15**, 148–166 (2022).
35. Kangani, M., Hazeri, N. & Maghsoodlou, M. T. A mild and environmentally benign synthesis of tetrahydrobenzo [b] pyrans and pyrano [c] chromenes using pectin as a green and biodegradable catalyst. *J. Chin. Chem. Soc.* **63**, 896–901 (2016).
36. Saadati-Moshtaghin, H. R. & Zonoz, F. M. Preparation and characterization of magnetite-dihydrogen phosphate as a novel catalyst in the synthesis of tetrahydrobenzo [b] pyrans. *Mater. Chem. Phys.* **199**, 159–165 (2017).
37. Elhamifar, D., Ramazani, Z., Norouzi, M. & Mirbagheri, R. Magnetic iron oxide/phenylsulfonic acid: A novel, efficient and recoverable nanocatalyst for green synthesis of tetrahydrobenzo [b] pyrans under ultrasonic conditions. *J. Colloid Interface Sci.* **511**, 392–401 (2018).
38. Norouzi, M., Elhamifar, D., Mirbagheri, R. & Ramazani, Z. Synthesis, characterization and catalytic application of a novel ethyl and boron sulfonic acid based bifunctional periodic mesoporous organosilica. *J. Taiwan Inst. Chem. Eng.* **89**, 234–244 (2018).
39. Shaker, M. & Elhamifar, D. Magnetic Ti-containing phenylene-based mesoporous organosilica: A powerful nanocatalyst with high recoverability. *Colloids Surf. A Physicochem. Eng. Aspects* **608**, 125603 (2021).
40. Zhang, L.-Y. *et al.* Control synthesis of magnetic Fe_3O_4–chitosan nanoparticles under UV irradiation in aqueous system. *Curr. Appl. Phys.* **10**, 828–833 (2010).
41. Norouzi, M. & Elhamifar, D. Ionic liquid-modified magnetic mesoporous silica supported tungstate: A powerful and magnetically recoverable nanocatalyst. *Compos. Part B Eng.* **176**, 107308 (2019).
42. Karimi, B., Maleki, A., Elhamifar, D., Clark, J. H. & Hunt, A. J. Self-assembled organic–inorganic hybrid silica with ionic liquid framework: A novel support for the catalytic enantioselective Strecker reaction of imines using Yb (OTf) 3–pybox catalyst. *Chem. Commun.* **46**, 6947–6949 (2010).
43. Mirbagheri, R. & Elhamifar, D. Magnetic ethyl-based organosilica supported Schiff-base/indium: A very efficient and highly durable nanocatalyst. *J. Alloys Compd.* **790**, 783–791 (2019).
44. Kargar, S., Elhamifar, D. & Elhamifar, D. Ionic liquid/high-density polyethylene composite supported molybdenum complex: A powerful, highly stable and easy recoverable catalyst. *J. Polym. Res.* **29**, 484 (2022).
45. Li, W., Zhang, B., Li, X., Zhang, H. & Zhang, Q. Preparation and characterization of novel immobilized Fe_3O_4@SiO_2@ mSiO_2–Pd (0) catalyst with large pore-size mesoporous for Suzuki coupling reaction. *Appl. Catal. A Gen.* **459**, 65–72 (2013).
46. Hou, S. *et al.* Synthesis of core–shell structured magnetic mesoporous silica microspheres with accessible carboxyl functionalized surfaces and radially oriented large mesopores as adsorbents for the removal of heavy metal ions. *RSC Adv.* **7**, 51993–52000 (2017).

47. Zhang, Y. *et al.* Benzoboroxole-functionalized magnetic core/shell microspheres for highly specific enrichment of glycoproteins under physiological conditions. *Small* **10**, 1379–1386 (2014).
48. Liu, G., Wang, D., Zhou, F. & Liu, W. Electrostatic self-assembly of Au nanoparticles onto thermosensitive magnetic core-shell microgels for thermally tunable and magnetically recyclable catalysis. *Small* **11**, 2807–2816 (2015).
49. Wang, Y. *et al.* Highly selective fluorescent chemosensor for Zn^{2+} derived from inorganic-organic hybrid magnetic core/shell Fe_3O_4@SiO_2 nanoparticles. *Nanoscale Res. Lett.* **7**, 1–13 (2012).
50. Lee, J. *et al.* Simple synthesis of functionalized superparamagnetic magnetite/silica core/shell nanoparticles and their application as magnetically separable high-performance biocatalysts. *Small* **4**, 143–152 (2008).
51. Sing, K., Everett, D., Raw, H. & Ra, R. J. & Siemieniewska, T. Reporting physisorption data for gas/solid system with special reference to the determination of surface area and porosity. *Pure Appl. Chem.* **57**, 603–619 (1985).
52. Abaeezadeh, S., Elhamifar, D., Norouzi, M. & Shaker, M. Magnetic nanoporous MCM-41 supported ionic liquid/palladium complex: An efficient nanocatalyst with high recoverability. *Appl. Organomet. Chem.* **33**, e4862 (2019).
53. Alinezhad, H., Tarahomi, M., Maleki, B. & Amiri, A. SO3H-functionalized nano-MGO-D-NH2: Synthesis, characterization and application for one-pot synthesis of pyrano [2, 3-d] pyrimidinone and tetrahydrobenzo [b] pyran derivatives in aqueous media. *Appl. Organomet. Chem.* **33**, e4661 (2019).
54. Khazaei, A., Gholami, F., Khakyzadeh, V., Moosavi-Zare, A. R. & Afsar, J. Magnetic core–shell titanium dioxide nanoparticles as an efficient catalyst for domino Knoevenagel–Michael-cyclocondensation reaction of malononitrile, various aldehydes and dimedone. *RSC Adv.* **5**, 14305–14310 (2015).
55. Mane, V. U., Chavan, S. M., Choudhari, B. & Mane, D. V. Microwave assisted synthesis of tetrahydrobenzo [b] pyrans via one pot multicomponent reaction using $[Et_3NH][HSO_4]$ as ionic liquid catalyst. *J. Pharm. Chem. Biol. Sci.* **6**, 311–319 (2019).
56. Sameri, F., Mobinikhaledi, A. & Bodaghifard, M. A. Preparation of core/shell CaO@SiO_2-SO_3H as a novel and recyclable nanocatalyst for one-pot synthesize of dihydropyrano [2, 3-c] pyrazoles and tetrahydrobenzo [b] pyrans. *Silicon*, **14**, 1–12 (2021).
57. Ataie, F., Davoodnia, A. & Khojastehnezhad, A. Graphene oxide functionalized organic-inorganic hybrid (GO–Si–NH_2–PMo): An efficient and green catalyst for the synthesis of tetrahydrobenzo [b] pyran derivatives. *Polycycl. Aromat. Compds.* **41**, 781–794 (2021).
58. Taheri, K., Elhamifar, D., Kargar, S. & Zarnegaryan, A. Graphene oxide supported ionic liquid/Fe complex: A robust and highly stable nanocatalyst. *RSC Adv.* **13**, 16067–16077 (2023).

Acknowledgements

The authors thank the Yasouj University and the Iran National Science Foundation (INSF) for supporting this work.

Author contributions

F.D.: writing—original draft, investigation, resources, formal analysis. D.E.: Conceptualization, writing—review and editing, supervision, visualization. All authors reviewed the manuscript.

Competing interests

The authors declare no competing interests.

Additional information

Correspondence and requests for materials should be addressed to D.E.

Reprints and permissions information is available at www.nature.com/reprints.

Publisher's note Springer Nature remains neutral with regard to jurisdictional claims in published maps and institutional affiliations.